SUPPORTING INFORMATION

Experimental Materials and Methods with Extended Discussion, Figures S1-S10, Table S1, and Supplementary References

Experimental Materials and Methods with Extended Discussion

Preparation of RNA. RNA oligonucleotides for solution and crystallography studies were obtained by chemical synthesis (Integrated DNA Technologies, Coralville, IA) and purified by desalting. Stock solutions were prepared by dissolving lyophilized single stranded oligonucleotides in 10mM sodium cacodylate buffer, pH 6.5.

Double-stranded RNA for solution studies was annealed from stoichiometric amounts of single-stranded stock solutions in the presence of 5mM $MgCl_2$ by heating to 65°C for 5 minutes followed by snap cooling and incubation at 4°C for 5 minutes. Double-stranded RNA for crystallographic studies was annealed in the same way but in the absence of $MgCl_2$ and by slow cooling to room temperature over 45 minutes. For programmable large triangle solution studies, corners A, B, and C were assembled individually by annealing stoichiometric amounts of single-stranded stock solutions in the presence of 5mM $MgCl_2$ by heating to 65°C for 5 minutes followed by snap cooling and incubation at 4°C for 5 minutes. Equal volume amounts of corners A, B, and C were then mixed and incubated at 25°C or 37°C for 20 minutes to assemble ABC programmable large triangles.

Gel Electrophoresis. RNA solution structures were analyzed on 13% native polyacrylamide gels in 2X MOPS buffer, pH 7.0 (40mM 3-morpholinopropane-1-sulfonic acid, 10mM sodium acetate) and corresponding $MgCl_2$ concentration at 4°C. RNA was visualized by staining with ethidium bromide and illumination under UV. Single-stranded RNA (inner, outer alone) was loaded at 1.5X concentration of double-stranded RNA (both; Figures 2 and S4) for greater band staining intensity with ethidium bromide. Size reference markers were a low range single-stranded RNA ladder (New England Biolabs, Ipswich, MA).

Thermo- and Chemical Stability. To test for resistance to boiling temperatures and chemical denaturation, assembled RNA nanotriangles were incubated at 25°C or 100°C in the presence or absence of 8M urea for 5 minutes. Samples were then immediately frozen on dry ice to prevent the reassembly of dissociated RNA nanotriangles, where they remained until loaded on a gel at 4°C.[21]

Extended Discussion of Thermo- and Chemical Stability. After 5 minutes incubation at 100°C, the assembled small triangle was recovered largely intact (~70%; Figure 2b, top, well 4), with slightly less recovery (~65%; Figure 2b, bottom, well 4) of the assembled large triangle. Similarly, after 5 minutes incubation with 8M urea at room temperature, the small and large triangles were mostly intact (~60 and ~75% recovery, respectively; Figure 2b, well 3). Boiling in the presence of 8M urea led to lower recovery of the small and large triangles (~40% and ~50%, respectively; Figure 2b, well 5).

RNA Assembly and Dissociation in Presence of Switch-Binding Ligand. RNA nanotriangle assembly in the presence of switch-binding or control ligands was measured by annealing stoichiometric amounts of single-stranded RNA in the presence of 5mM $MgCl_2$, with 0, 100, or 500uM switch-binding benzimidazole ligand[20] or control ligands by heating to 65°C for 5 minutes followed by snap cooling and incubation at 4°C for 5 minutes. Dissociation of already assembled RNA nanotriangles was measured when incubated at 25°C or 37°C for 20 minutes in the presence of 0, 100, or 500uM switch-binding ligand.

Crystallization, Data Collection, and Structure Determination. SVV IIa short and long RNA crystal structures were obtained as described earlier.[16] Assembled RNA

nanotriangles were crystallized at 6°C by hanging drop vapor diffusion. In crystallization setups, 1µL of 0.2mM RNA was mixed with an equal volume of precipitant solution containing 55mM NaCl, 12mM spermine, 40mM Tris hydrochloride buffer, pH 7.5, and 20% methyl-2,4-pentanediol (MPD). Crystals grew over the course of one month of equilibration against 700µL of well solution containing 120mM NaCl and 18% MPD.

Crystals were flash-cooled in liquid nitrogen. X-ray diffraction data were collected at 110K on a Rigaku rotating anode X-ray generator (λ = 1.54 Å) equipped with a MAR345 imaging plate detector system. Datasets were processed, integrated, and scaled with the HKL2000 package.[22] The three-dimensional structure of the RNA nanotriangle was solved by molecular replacement with the program Phaser[23] using search models derived from the short and long SVV IIa RNA crystal structures (RCSB Protein Data Bank accession codes 4P97 and 4PHY), and refined by the program Refmac[24] both within the CCP4 package.[25] Subsequent iterative rounds of manual building and refinement, alternating between Refmac and manual rebuilding in Coot,[26] were based on the obtained 2Fo-Fc and Fo-Fc maps. Chloride ions were assigned based on electron density, B-factor refinement and distance as well as geometry of coordinating ligands. Final refinement was carried out in PHENIX[27] with individual isotropic atomic displacement parameters and water picking (Table S1). Coordinates and structure factors have been deposited in the RCSB Protein Data Bank under accession code 5CNR.

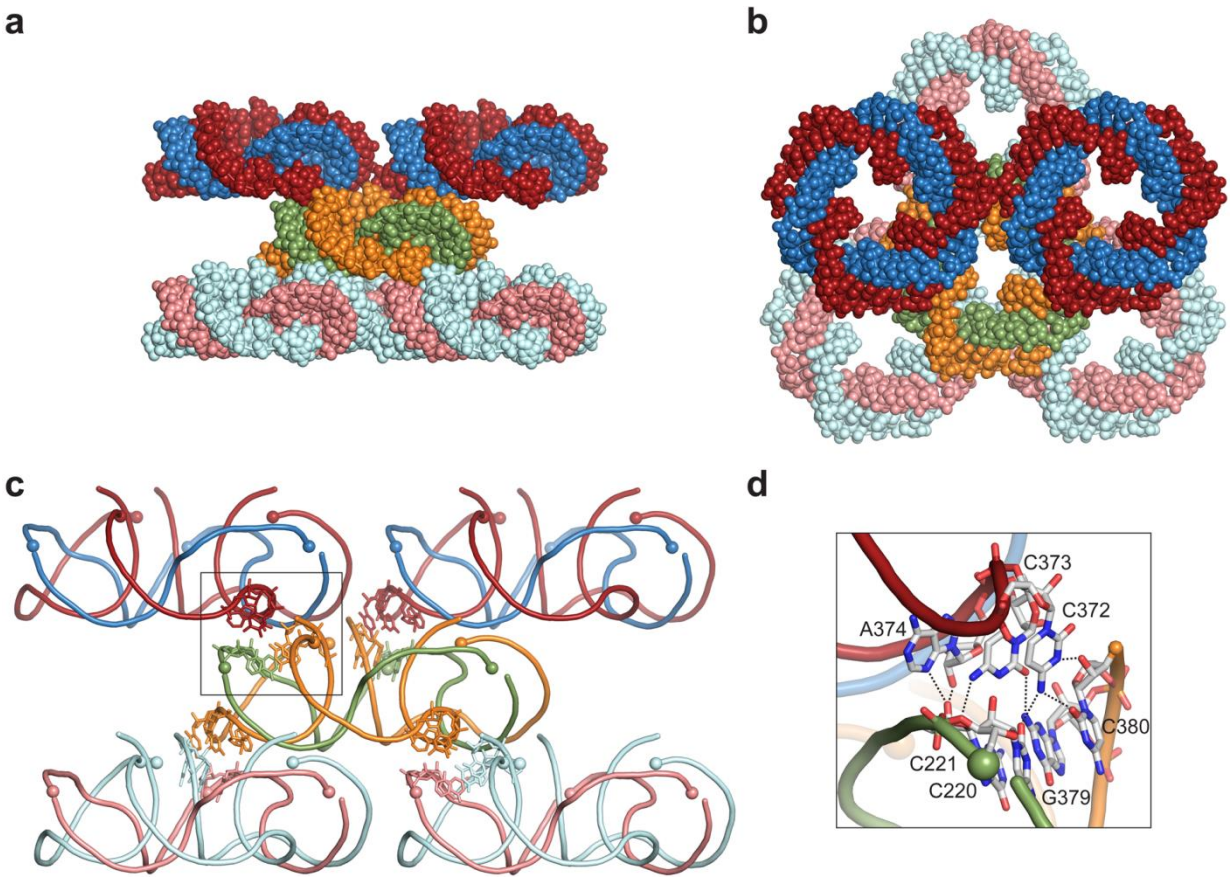

Figure S1. Crystal packing of pseudo-continuously closed triangles in the subdomain IIa short oligonucleotide construct (see Figure 1a). a) Side view of triangle layers. b) Top-down view reveals triangles arranged in a pattern that repeats every three layers. c) Layers contain triangles facing in the same direction. Residues that are involved in hydrogen bonding contacts between layers are shown in stick representation. 5′ termini of oligonucleotides are indicated by spheres. d) Hydrogen bond interactions between both strands in one triangle (orange, green) and the outer strand (red) of the overlaying triangle. In total, 18 hydrogen bonds form across the interface of one triangle with three overlaying triangles.

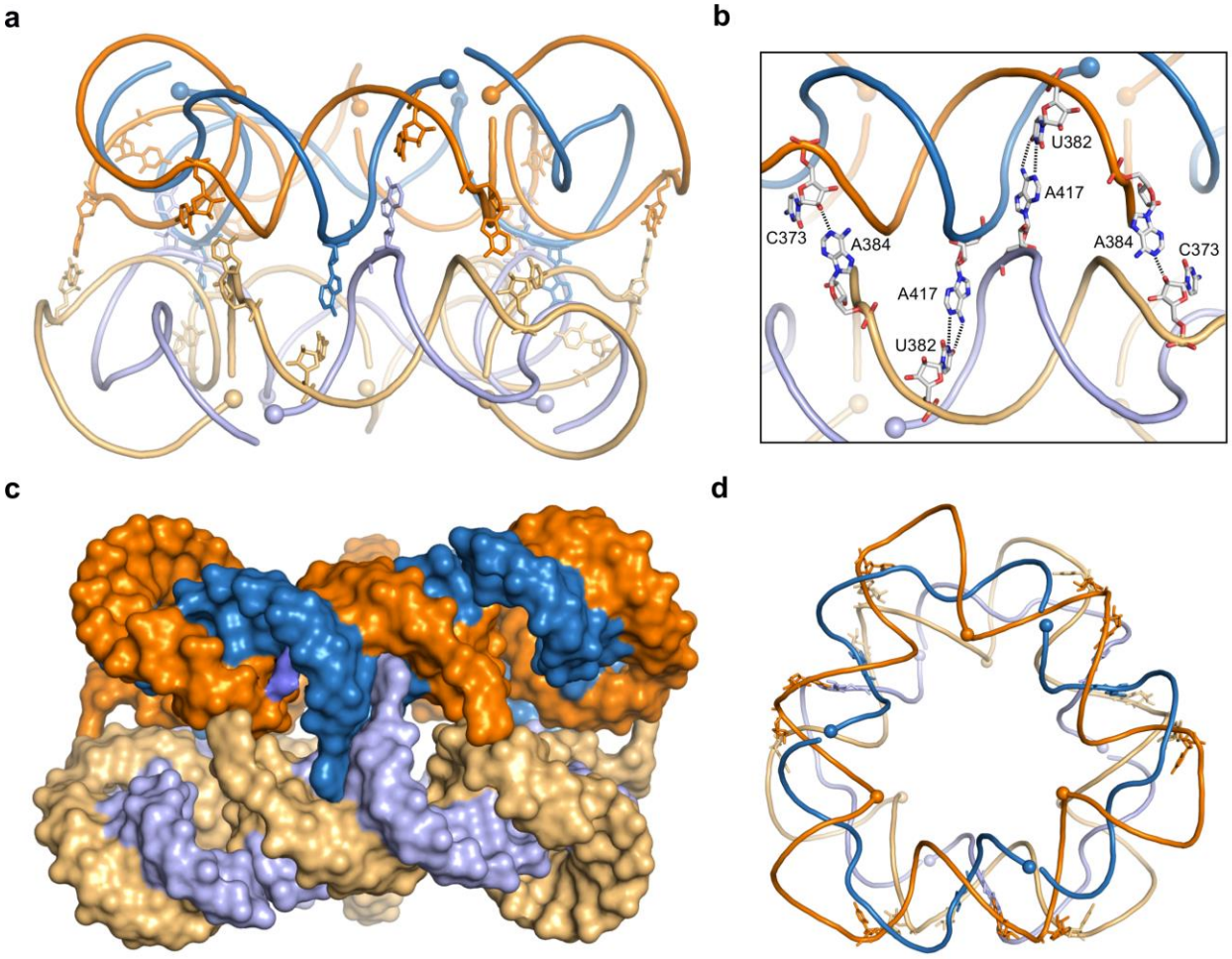

Figure S2. Face-to-face dimer formation of pseudo-continuously closed large triangles in crystals of the subdomain IIa long oligonucleotide construct (see Figure 1a). Dimers involve 3 pairs of symmetrical A417-U382 Watson-Crick base pairs and 3 pairs of symmetrical A384○C373 hydrogen bonding interactions (panels a,b). In the A417-U382 interaction, the adenosine of one triangle replaces the dimer triangle's adenosine by reaching across to form a Watson-Crick base pair with the dimer triangle's uridine and stacks in between the neighboring base pairs without interrupting the RNA helix. A384 flips out and forms a hydrogen bond interaction with the unpaired C373 corner residue. a) Side view of triangle dimer packing interactions which involves 12 total base pair interactions. Outer strands are shown in orange hues and inner strands are shown in blue/violet hues. b) The packing of each triangle side consists of two symmetrical A417-U382 Watson-Crick base pairs and two symmetrical A384○C373 base pairs in which the cytosine 2′OH group forms a hydrogen bond with the Watson-Crick edge of the adenosine. c) Side-view surface representation of dimer showing

unique cross-over base pairing interactions between triangles. d) Top-down view of triangle dimers.

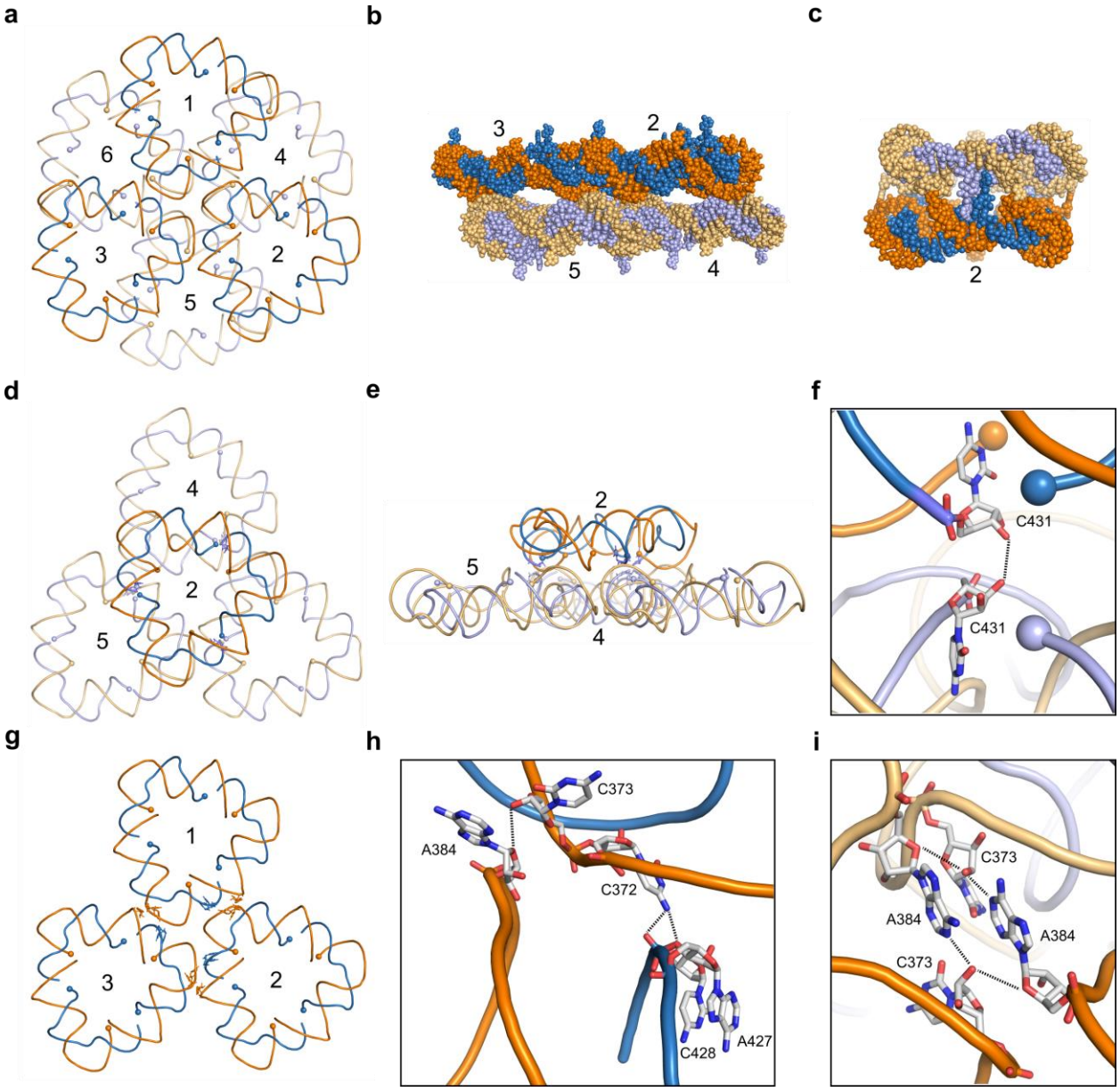

Figure S3. End-to-end and side-to-side packing of pseudo-continuously closed large triangles in crystals of the long subdomain IIa oligonucleotide construct (see Figure 1a). Outer strands are shown in orange hues and inner strands are shown in blue/violet hues. a) Top down view of two layers of end-to-end crystal packing not involved in dimer formation. b) Side view of end-to-end packing shown in panel a. c) Side view of triangle dimer (Figure S2c) involving triangle 2 and a triangle in the layer above it. d) Shifted top down view of triangle 2 interacting in an end-to-end fashion with the layer beneath it. Triangles 4 and 5 can also be seen in panel a. e) Side view of end-to-end packing shown in panel d. f) Single hydrogen bond formation between the C431 of

triangle 2 and the C341 of each of the 3 triangles beneath 2. g) Top down view of triangles packing side-to-side. h) Hydrogen bonds formed between triangles within a layer. Each triangle forms a total of 18 hydrogen bonds with the surrounding six triangles within a layer. i) Hydrogen bond and packing interactions involving two A384○C373 pairs involved in dimer formation (see panel c and Figure S2b) and side-to-side interactions (see panel h).

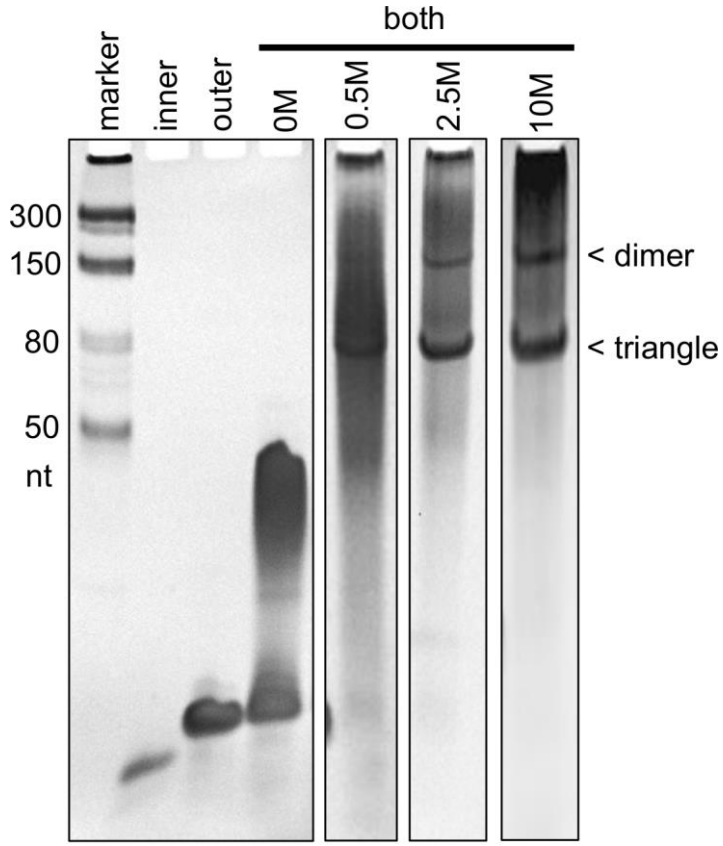

Figure S4. Magnesium ion concentration dependence of large nanotriangle self-assembly and formation of major and minor band species analyzed by 13% native polyacrylamide gel electrophoresis (PAGE) with 0, 0.5, 2.5, or 10mM $MgCl_2$. Each box shows results from separate gel experiments. The corresponding magnesium concentration used in the reaction, loading and running buffers, as well as the gel are indicated in the legend on top. A single-stranded RNA ladder was loaded on each gel as a reference marker but shown only for the left-most gel. At 0M $MgCl_2$ major or minor band formation is not observed. At 0.5M $MgCl_2$ the major and minor band formed at a 10:1 ratio. At 2.5M $MgCl_2$ the major and minor band formed at a 1.7:1 ratio. At 10M $MgCl_2$ the major and minor band formed at a 1.3:1 ratio.

The faster moving major band was confirmed as a single triangle of three corners by comparative analysis of a programmable triangle with three distinct corners (see discussion in main text and Figure 2d). The minor band migrates at a slower speed consistent with a species roughly twice the size of a single triangle. This minor band is formed by both the symmetrical and programmable small triangles (see Figures 2, S4, and S6), and is likely a dimer of triangles

or a nonplanar hexagon with A-B-C-A-B-C configuration. Face-to-face dimer formation of pseudo-continuously closed large triangles involving 12 total base pair interactions was seen in the crystal structure packing of the long SVV IIa construct (Figure S2), and may be similar to the interactions causing the slower moving minor band for the large triangle in solution.

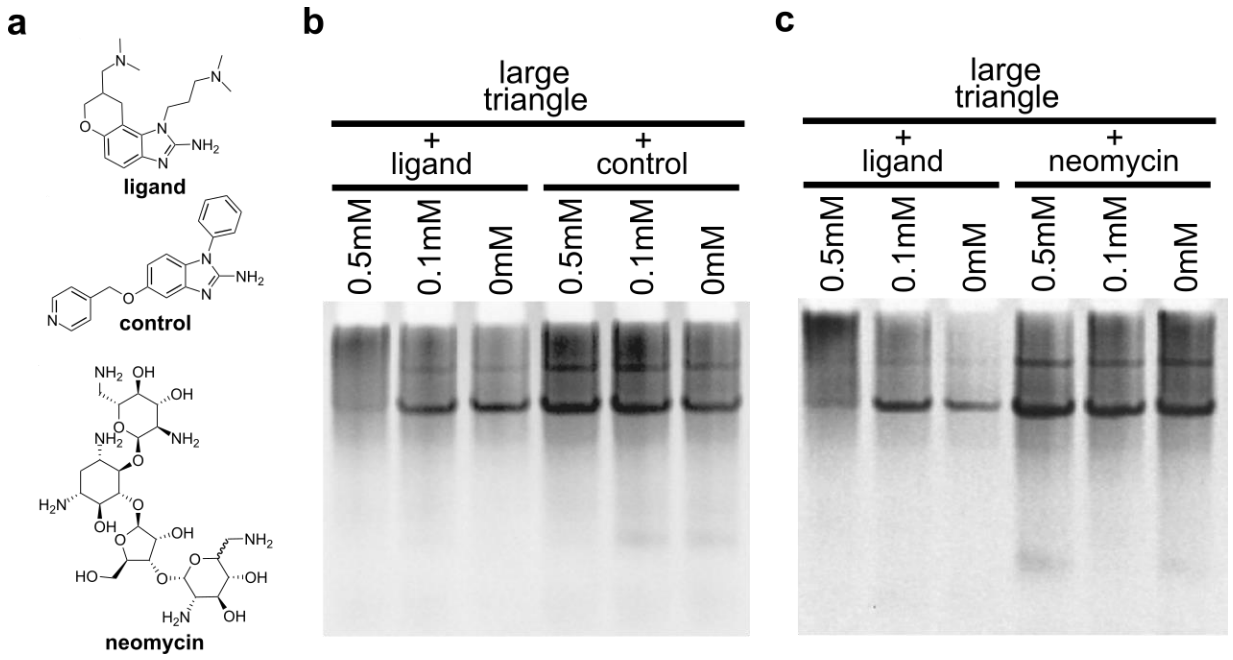

Figure S5. Large nanotriangle self-assembly efficiency in the presence of a binding ligand and control compounds. a) Structures of the benzimidazole ligand which binds to the IIa RNA switch element of the nanotriangles, the structurally related but non-binding aryl-substituted benzimidazole control, and the non-specific RNA binder neomycin. b) Large triangle assembly was disrupted only by specific IIa-switch binding benzimidazole ligand and not by a related control compound which was found to be inactive in a target-specific FRET binding assay.[28] c) Neomycin, an aminoglycoside which binds structured RNA promiscuously, also showed no effect on large triangle assembly.

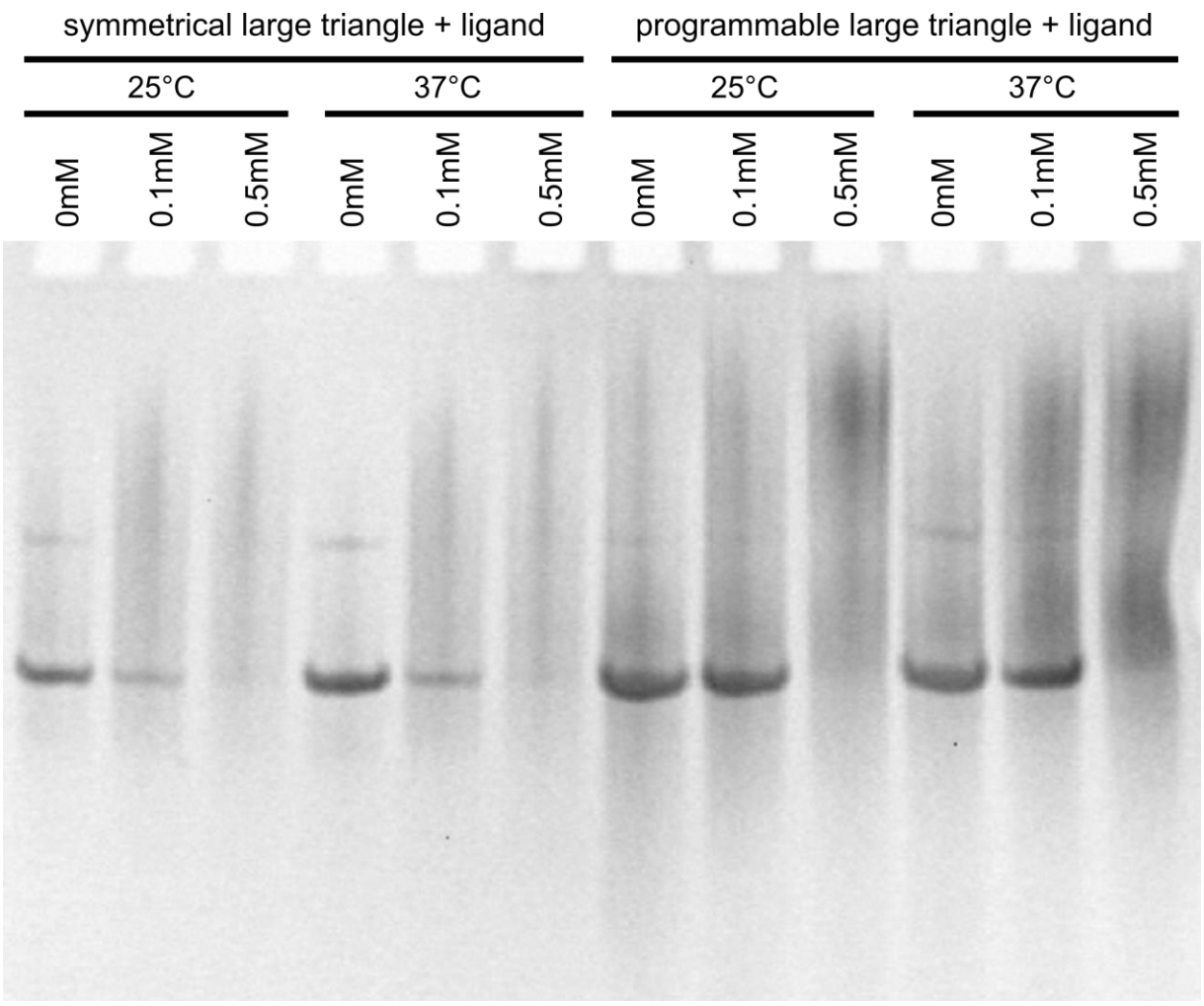

Figure S6. Dissociation of symmetrical and programmable large nanotriangles was observed when incubated post-assembly with 100 or 500μM benzimidazole ligand (Figure S5a) for 20 minutes at 25°C or 37°C.

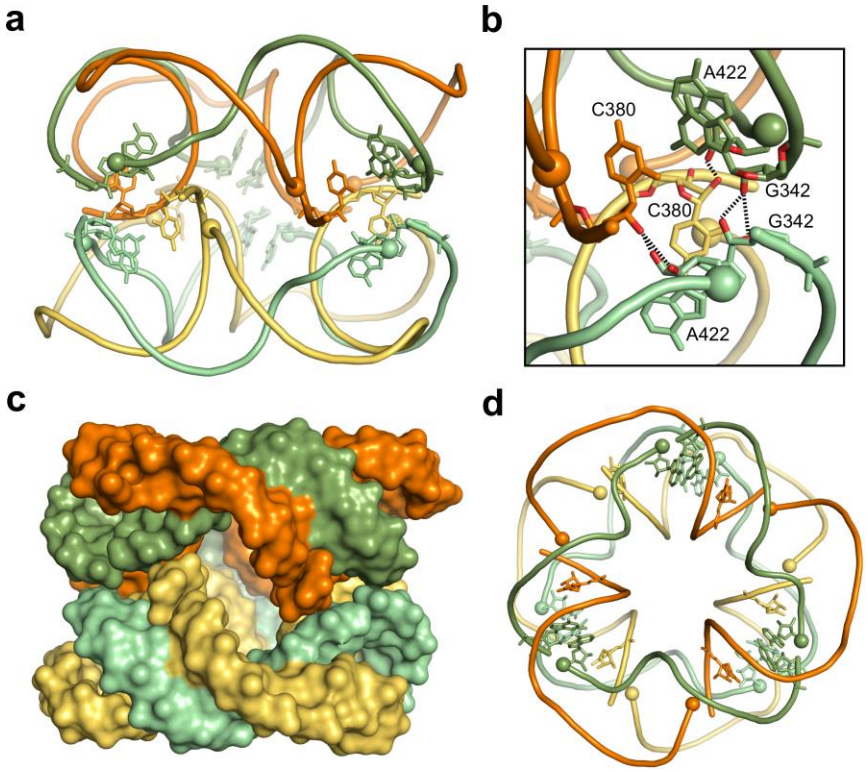

Figure S7. In the intermolecular packing of the crystal structure, the RNA nanotriangle forms face-to-face dimers. These triangle packing dimers form 15 intermolecular hydrogen bond contacts in addition to having complementary surface shapes that maximize packing. a) Two RNA triangles pack facing each other with the side that carries the oligonucleotide termini. Residues that are involved in hydrogen bonding contacts between triangles are shown in stick representation. 5′ ends are marked by spheres. b) Hydrogen bond interactions between the sugars of two different C380○A422 pairs separated by the hydrogen bond interactions between the sugars of two G342 residues at the strand termini of the upper (orange, green) and lower (yellow, teal) triangle at the dimer interface. In total, 15 hydrogen bonds form across the packing interface of two triangles. c) Shape complementarity at the interface of RNA triangle dimers maximizes packing surface contacts. The sugar phosphate backbone at the termini of the outer strands in the upper triangle (orange) is fitted into the major groove of the bend in the outer strand of the lower triangle (yellow). d) Top down view of a dimer showing the backbone-into-groove fitting between outer strands of the upper and lower RNA triangles.

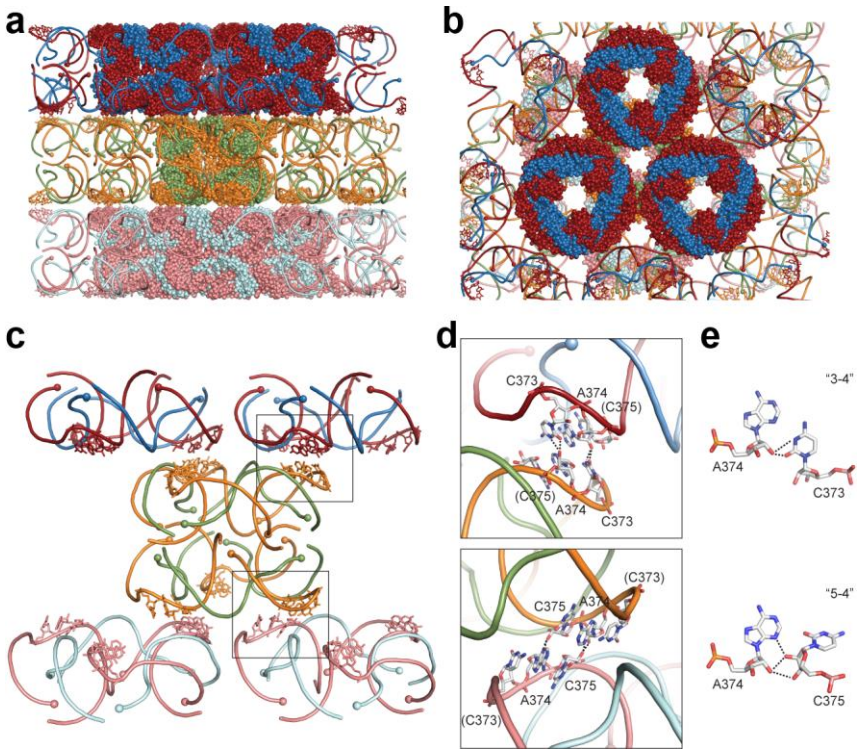

Figure S8. In the extended crystal packing, triangle dimers form layers that stack in alternating orientations. While no direct lateral hydrogen bond interactions are formed within layers, alternating dimer layers form hydrogen bond contacts with neighboring layers in one of two distinct ways which involve residues C373, A374, and C375 and alternate with each additional layer. a) Face-to-face triangle dimers form layers. Outer strands are shown in red/orange hues and inner strands in blue/green color. b) Consecutive layers of face-to-face triangle dimers stack in an alternating fashion. c) Packing contacts occur between dimer layers and involve RNA outer strands only. Lateral contacts between triangles within layers are not observed. d) Residues C373, A374 and C375 participate in packing interactions mediated by two distinct patterns of hydrogen bonding (indicated by boxes in panel c). e) The "3-4" pattern consists of two symmetrical C373○A374 base pairs in which the Watson-Crick edge of the cytidine forms two hydrogen bonds with the 2′OH group of the adenosine. The "5-4" motif includes two symmetrical C375○A374 pairs in which the cytosine ribose engages in three hydrogen bonds with the sugar edge of the adenosine.

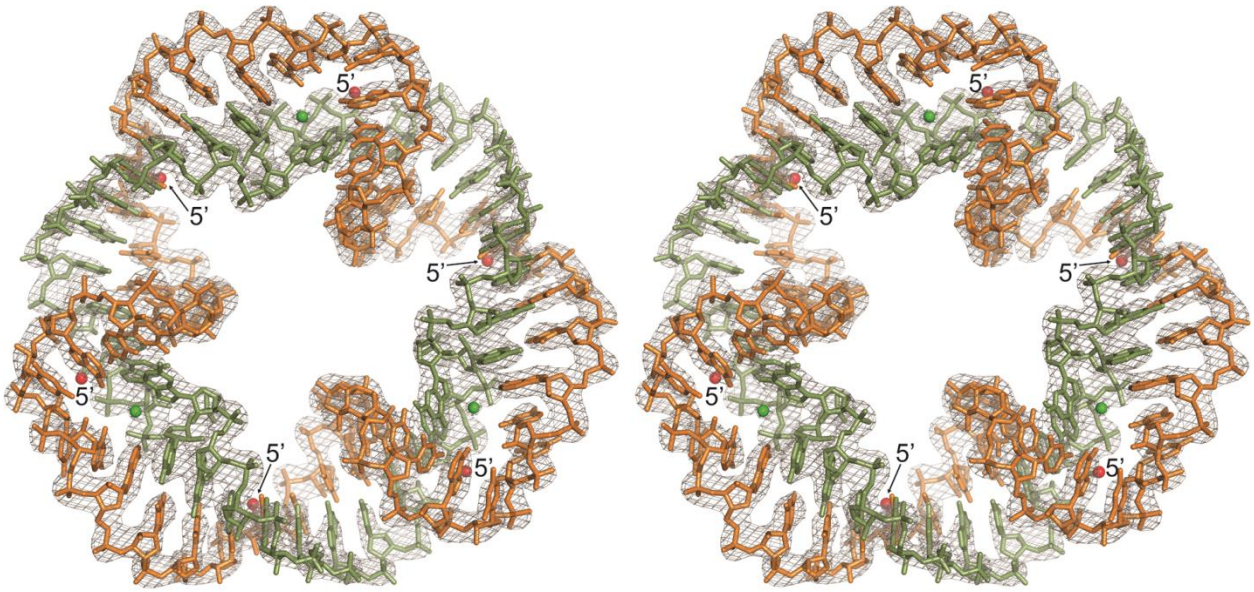

Figure S9. Stereo view of the crystal structure and electron density map ($2F_o$-F_c, contoured at 2.0 σ) of the self-assembling RNA nanotriangle. Positions of oligonucleotide 5′ termini are indicated by red spheres. While triangle self-assembly in solution was dependent on magnesium ion concentration, cations were not observed in the crystal structure, but three chloride anions per triangle were found at the Watson-Crick edge of A374 and C375 (green spheres) and supported by electron density and coordination environment. Similarly, magnesium ions were not observed in the short SVV IIa construct crystal that shows the pseudo-continuously closed small triangle packing, although magnesium was required for its folding in solution.[16]

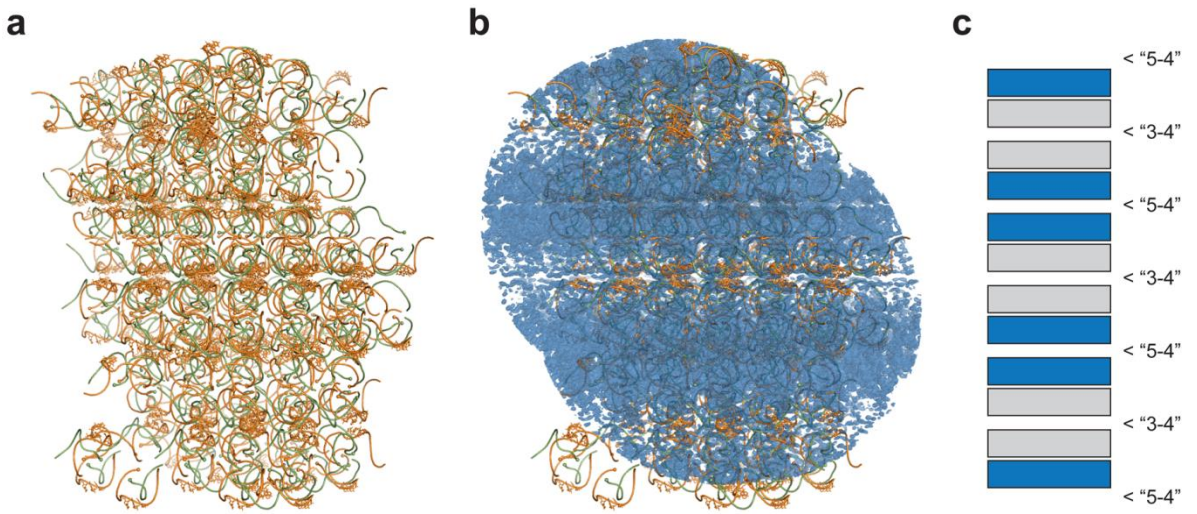

Figure S10. One-dimensional twinning disorder of crystal packing layers of the self-assembling RNA nanotriangle. a) Side view of six layers of RNA triangle face-to-face dimers. b) Electron density map ($2F_o$-F_c) around the six layers of RNA triangle dimers shown in panel a. Disordered layers are visible as stripes of low density (see discussion below). c) Arrangement of RNA triangle layers indicating disordered regions. Pairs of rectangles indicate face-to-face dimers of RNA triangles. Packing interactions between dimers are classified as "3-4" or "5-4" type, depending on the hydrogen bonding pattern (see Figure S8d,e). RNA triangles represented by blue rectangles are well ordered and completely covered by electron density while those indicated by grey rectangles are within disordered regions of non-continuous density.

The one-dimensional twinning disorder observed in the crystal packing gives rise to a regular pattern of weak electron density layers interspersed between well-defined regions. Stacking of consecutive layers of nanotriangles allows for several possible arrangements (see Figure S8) such that each successive layer may be displaced laterally relative to the one below it. Such twinning disorder occurs when successive planar crystal layers shift laterally into any of several alternative, energetically similar configurations. Weak stacking interactions between layers facilitate this type of twinning which has been investigated in detail by Trame and McKay[29] and was observed in other crystal structures, both of proteins (for example, Benirschke and coworkers)[30] and small molecules (for example, Schwarzenbach and coworkers).[31] As these authors pointed out, the regularity of the electron density in the ordered layers allows for

structure refinement to acceptable parameters. This is confirmed by the quality of parameters obtained for the RNA nanotriangle crystal structure (see Table S1).

Table S1. Crystallographic data collection and refinement statistics for the self-assembling RNA nanotriangle.

Data Collection	
Wavelength (Å)	1.54
High-resolution limit (Å)	2.60
Low-resolution limit (Å)	19.40
Redundancy[a]	17.6 (2.0)
Completeness (%)[a]	83.2 (11.7)
$I/\sigma(I)$[a]	35.53 (1.83)
Total reflections	88115
Unique reflections	5011
Refinement	
Space group	R32
Cell dimensions (Å)	
a	59.93
b	59.93
c	262.62
α	90
β	90
γ	120
R_{work}/R_{free}	0.19 / 0.24
No. atoms	
RNA atoms	1136
Ligand	Cl^-
Mean *B* factors (Å^2)	
RNA	152.1
Ligand	124.7
R.m.s. deviations	
Bond lengths (Å)	0.002
Bond angles (°)	0.445
Dihedral angles (°)	14.08

[a]Numbers in parentheses are for the highest-resolution shell.

Supplementary References

[21] E. F. Khisamutdinov, D. L. Jasinski, P. Guo, *ACS Nano* **2014**, *8*, 4771.

[22] Z. Otwinowski, W. Minor, *Methods Enzymol.* **1997**, *276*, 307.

[23] A. J. McCoy, R. W. Grosse-Kunstleve, P. D. Adams, M. D. Winn, L. C. Storoni, R. J. Read, *J. Appl. Crystallogr.* **2007**, *40*, 658.

[24] G. N. Murshudov, A. A. Vagin, E. J. Dodson, *Acta Crystallogr. Sect. D Biol. Crystallogr.* **1997**, *53*, 240.

[25] *Acta Crystallogr. D. Biol. Crystallogr.* **1994**, *50*, 760.

[26] P. Emsley, K. Cowtan, *Acta Crystallogr. Sect. D Biol. Crystallogr.* **2004**, *60*, 2126.

[27] P. D. Adams, R. W. Grosse-Kunstleve, L. W. Hung, T. R. Ioerger, A. J. McCoy, N. W. Moriarty, R. J. Read, J. C. Sacchettini, N. K. Sauter, T. C. Terwilliger, *Acta Crystallogr D Biol Crystallogr* **2002**, *58*, 1948.

[28] K. Ding, A. Wang, M. A. Boerneke, S. M. Dibrov, T. Hermann, *Bioorg. Med. Chem. Lett.* **2014**, *24*, 3113.

[29] C. B. Trame, D. B. McKay, *Acta Crystallogr. Sect. D Biol. Crystallogr.* **2001**, *57*, 1079.

[30] R. C. Benirschke, J. R. Thompson, Y. Nominé, E. Wasielewski, N. Juranić, S. Macura, S. Hatakeyama, K. I. Nakayama, M. V. Botuyan, G. Mer, *Structure* **2010**, *18*, 955.

[31] D. Schwarzenbach, K. Kirschbaum, A. A. Pinkerton, *Acta Crystallogr. B.* **2006**, *62*, 944.